

SUPPLEMENTARY MATERIALS

This supplement is subdivided into four parts that contain information on the sample locations, biostratigraphic assignments, U-Pb methods and results, and the $^{40}\text{Ar}/^{39}\text{Ar}$ methods and results.

Note that Table DR 4.2 with the complete $^{40}\text{Ar}/^{39}\text{Ar}$ results from samples and neutron fluence monitors is provided as an excel spreadsheet file at the end of this supplement.

<u>Table of contents</u>	<u>Page</u>
<u>Part 1. Sample locations and descriptions.</u>	
Table DR 1.1. Detailed locations and descriptions of dated ash beds.	2
Figure DR 1.2. Coniacian-Santonian paleogeographic map with sample locations.	3
<u>Part 2. Detailed biostratigraphic appendix DR2.</u>	4
<u>Part 3. U-Pb zircon geochronology.</u>	
Section DR 3.1. U-Pb methods and data interpretation.	9
Figure DR 3.2. Cathodoluminescence images of selected zircons or fragments.	11
Table DR 3.3. U-Pb isotope data from analyzed zircons in Cretaceous ash beds.	13
Section DR 3.4. ^{238}U - ^{206}Pb and $^{40}\text{Ar}/^{39}\text{Ar}$ data pairs.	14
Table DR 3.5. Table of age differences between ^{238}U - ^{206}Pb and $^{40}\text{Ar}/^{39}\text{Ar}$ data pairs.	16
Figure DR 3.6. Probability of fit for various combinations of ^{238}U - ^{206}Pb zircon dates.	17
Figure DR 3.7. Concordia plots of U-Pb zircon analyses and $^{206}\text{Pb}/^{238}\text{U}$ dates.	18
<u>Part 4. $^{40}\text{Ar}/^{39}\text{Ar}$ sanidine geochronology.</u>	
Section DR 4.1. $^{40}\text{Ar}/^{39}\text{Ar}$ methods.	19
Table DR 4.2. Complete $^{40}\text{Ar}/^{39}\text{Ar}$ isotope data from samples and standard minerals used as neutron fluence monitors.	21
Figure DR 4.3. Age spectrum diagrams from incremental heating analyses.	21
<u>Part 5. References cited in Supplementary Materials.</u>	22

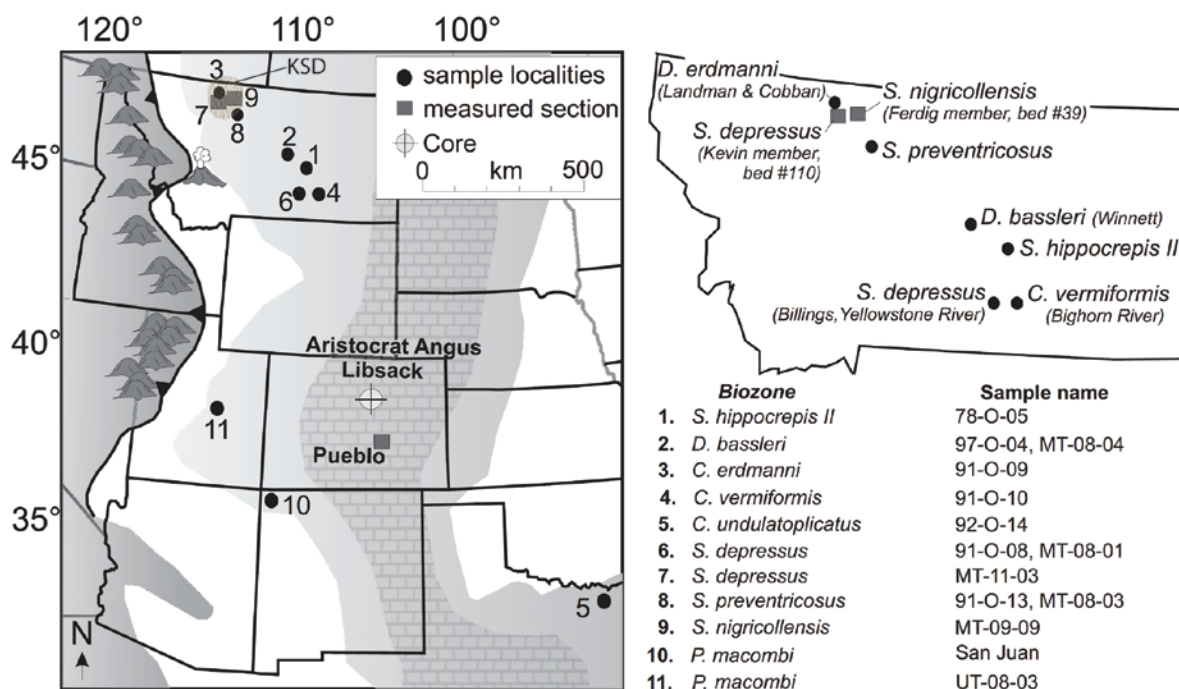
PART 1. LOCATIONS AND DESCRIPTIONS OF DATED ASH BEDS.

Table DR. 1.1. Detailed locality data for sampled ashes keyed to locality map (Fig. DR 1).

Biozone ¹	State	County	Latitude (N)	Longitude (W)	masl	Obradovich sample number	Obradovich 1993 site#	UW sample number	Sample description	Site #, this study
<i>Scaphites hippocrepis</i> II	MT	Petroleum	46.8800	107.8700		78-O-05	10	MT-08-02	sample is mis-located in Obradovich (1993). Correct location is in Cat Creek Anticline.	1
<i>Desmoscapites bassleri</i>	MT	Petroleum	47.0044	108.3340		97-O-04	11	MT-08-04	12 cm thick, grey to yellow orange bentonite near base of escarpment along east bank McDonald Creek. Overlain by 6 cm of carbonate and chert, black shale below. Contains both sandine and zircon.	2
<i>Desmoscapites erdmanni</i>	MT	Toole	48.4923	112.0303		91-O-09	none	MT-09-08 ns	Collected at site of <i>erdmanni</i> fossil locality #21419 in Landman and Cobban (2007). Equivalent to the 3 cm thick bentonite at the top of bed #187 of Kevin Member of the Marias River Formation (Cobban et al., 1976). Head of ravine, 12.9 km west of Shelby, MT. Sandines were purified from sample prepared by Obradovich, but not previously analyzed.	3
<i>Clioscapites vermiformis</i>	MT	Bighorn	45.721608	107.578755	907	90-O-10	none	MT-09-07 ns	4 inch thick bentonite collected by W. Cobban and A. Merewether on June 17, 1990 from cut bank on East side of Bighorn River, 1.35 miles southeast of Hardin, MT. Cobban's field notes from 1947 indicate that this bentonite is bed #112 in the section and crops out less than 1 meter below the <i>C. vermiformis</i> fossil locality #20953 (original field notes #478-118). Sandines were purified from sample originally prepared by Obradovich, but not previously analyzed.	4
<i>Cladoceramus undulaticollicatus</i>	TX	Grayson	33.5200	96.4034	220	92-O-14	13	not sampled in this study	Bentonite collected by W. Cobban and J. Obradovich at top of <i>I. undulaticollicatus</i> zone, presumably equivalent to 91 cm thick bentonite that yielded sample 86-O-15 of Obradovich (1993). Austin chalk in creek 1.1 km northwest of downtown White Wright, TX.	5
<i>Scaphites depressus</i>	MT	Toole	48.8172	112.0015	1122	none	none	MT-11-03	Bed #110 in Kevin Member of Marias River Shale Formation of Cobban et al. (1976). Collected by Singer and Guy Plint, August 2011.	7
<i>Scaphites depressus</i>	MT	Yellowstone	45.7407	108.5119	946	91-O-08	14	MT-08-01	30 cm thick, orange clay grades upward into grey clay, has thin red layers; capped with 10 cm thick bed of massive, blocky, fossil-rich silt; sits on black shale. Escarpment south of Billings, MT along Yellowstone River.	6
<i>Scaphites preventricosus</i>	MT	Toole	48.4288	111.8921	891	91-O-13	15	MT-08-03A	MT-08-03A is 20 cm thick bentonite sampled in Marias River Formation shales along north bank of Marias River, 0.5 km west of Interstate Highway 25. It is likely that sample 91-O-13 is from a bentonite within less than 1 meter above this sample.	8
<i>Scaphites nigrocollensis</i>	MT	Toole	48.8177	111.8156	1066	none	none	MT-09-09	Possibly equivalent to marker bed #39 in Ferdig Member of Marias River Formation of Cobban et al. (1976). Collected in the area of Ferdig type section, approx. 14 km east of main outcrops comprising Kewin type section of Cobban et al. (1976).	9
<i>Phyonocylus macombi</i>	UT	Emery	39.2226	110.9486	1747	SAN JUAN	16	UT-08-03	40 cm thick bentonite with crystal-rich base from this ammonite zone was collected in NM by J. Fassett and labeled "SAN JUAN" in Obradovich collection; sandine age was reported in Obradovich (1993). Our sample, collected from the <i>P. macombi</i> zone of the Ferron SS section of Gardner (1995), near Castle Dale, UT is most likely not at the same level within the <i>P. macombi</i> ammonite zone.	10,11

¹ Biozones from Scott and Cobban (1964), Cobban et al. (1976) and Cobban et al. (2006). Latitudes and Longitude reported in WGS-84 format from hand held GPS measurements; or located using GoogleEarth software. masl = meters above sea level

Figure DR 1.2. Coniacian-Santonian paleogeographic map of Western Interior region showing sample sites; inset of Montana state localities keyed to biozones. This map is Figure 1 from the text of the paper, repeated here for cross reference with Data Repository materials. The locations include: 1) Montana sites (1-4, 6-9) where most ash beds analyzed in this study were sampled (ashes from two biozones were sampled elsewhere, at sites 5, 10 and 11); (2) Montana measured sections of the Kevin and Ferdig Members of the Marias River Shale Formation (squares), based on Cobban et al. (1976); (3) Libsack and Aristocrat Angus boreholes in Colorado (circle with cross-hairs, representing location of both cores, drilled within 5 km of each other); and (4) measured section of the Niobrara Formation (square) near Pueblo, CO, based on Scott and Cobban (1964). The locality numbering scheme increases with age and stratigraphic depth; numbered ash layers were sampled within corresponding ammonite biozones, originally by Bill Cobban and colleagues, and resampled for this study. Obradovich (1993) samples re-analyzed in this study begin with his sample numbers (e.g., 97-O-04), whereas new UW-Madison samples begin with state abbreviations (e.g., MT-08-04). KSD=Kevin-Sunburst Dome. See Table DR 1.1 for corresponding details.



Part 2. Biostratigraphic Appendix DR2: Stratigraphic calibration, correlation of biozones and ashes.

This appendix documents the biostratigraphic data for each sampled ash, including the basis for biostratigraphic assignments in each section, and the basis of the MT-CO correlation for each biozone and dated ash shown in Figure 2 of the manuscript. The biozones are presented in ascending stratigraphic order (FAD = first appearance datum; LAD = last appearance datum).

Prionocyclus macombi – Ash beds were sampled in this zone at two localities in the central Western Interior to obtain a Late Turonian age constraint, but the zone is not identified in the Montana sections presented in this report. Locality details for sites #10 and #11 are summarized in Table DR 1.1, the localities are shown in Figure DR1.2, and corresponding geochronologic results are presented in Table 1 of the text.

Scaphites nigricollensis – This ash was sampled to obtain a Late Turonian age constraint as close as possible to the base of the Niobrara Formation. The sampled ash is from the Ferdig type section of Cobban et al. (1976) and occurs close to USGS Mesozoic locality 23666 containing *S. nigricollensis* (locality #9, Tab. DR1.1, Fig. DR1.2). Taxa representing this biozone do not occur in the Pueblo section, but this age date can be assigned to the hiatus at the base of the Fort Hays Member within which the zone occurs, as constrained by underlying (*Scaphites warreni*, *Prionocyclus macombi*, and *P. hyatti*, noted in Pueblo by Fisher et al., 1985) and overlying (*Mytiloides incertus*, *Mytiloides scupini*: Walaszczyk and Cobban, 2000) taxa.

Scaphites preventricosus – The base of the biozone in the Kevin Member is constrained by the first occurrence of *Cremonceramus deformis erectus*, which marks the base of the *Cremonceramus erectus* Zone that co-occurs commonly with *S. preventricosus*. Within a few meters upsection, fossils of *S. preventricosus* are found (USGS Mesozoic locality 20289; Cobban et al., 1976). The top of the biozone is constrained by the FAD of *Volviceramus* sp. just above

bed 55 in the Cobban et al. (1976) Kevin type section (Grifi et al., 2012), which also marks the base of middle Coniacian fauna and the base of the overlying *Scaphites ventricosus* biozone. The *preventricosus* ash was sampled in the Marias River section (Loc. #8, Tab. DR1.1, Fig. DR1.2) and correlated to bed 22 of the Kevin type section of Cobban et al. (1976); it occurs about midway through the biozone. The base and top of the *S. preventricosus* biozone in Pueblo are constrained by the FAD's of *Cremnoceramus deformis erectus* and *Volviceramus involutus*, respectively (Walaszczyk and Cobban, 2006), and the ash correlation is correspondingly placed midway between. The projection of the biozone and ash horizon to the Libsack core is based on lithostratigraphy (middle FHLS to top LSL). To account for possible correlation uncertainty a value equal to ± 0.5 of the biozone duration is applied.

Scaphites ventricosus – The base of the zone is defined by the FAD of *Volviceramus*, as described above, and the top of the zone is placed at the MacGowan bed (bed 100 of Cobban et al., 1976), a disconformity surface that omits much of the Middle Coniacian and possibly part of the Upper Coniacian. The upper boundary is constrained by the FAD of *Scaphites depressus* just above bed 100. No ash beds were sampled in the *ventricosus* zone.

Cladoceramus undulatoplicatus – A bentonite sample from the top of this inoceramid biozone, which coincides with the uppermost part of the *S. depressus* biozone, was collected by W. Cobban and J. Obradovich in the Austin Chalk, northeastern TX (see Tab. DR1.1). The sample yielded datable material and a new age based on re-analysis of legacy crystals is included in Figure 4 of the text.

Scaphites depressus – The base of the zone in the Kevin section is placed at the MacGowan hiatus and the top, defined by the FAD of *Clioscapites saxitonianus*, is just a few meters above. The base of the *Scaphites depressus* biozone is defined in Pueblo by the FAD of

Magadiceramus subquadratus (see Walaszczyk and Cobban, 2006), which was identified as *Inoceramus stantoni* (USGS Mesozoic locality D3473) by Scott and Cobban (1964). The top is constrained by the FAD of *Clioscaphtes saxitonianus* (USGS Mesozoic locality D3491: Scott and Cobban, 1964; see also Walaszczyk and Cobban, 2006). The Coniacian-Santonian boundary is placed at the FAD of *Cladoceramus undulatoplicatus* (see Walaszczyk and Cobban, 2006), which is in the topmost part of the *depressus* Zone. Comparison of the biozone from Pueblo to the Kevin type section indicates that much of the lower *depressus* zone is missing in the Kevin area. The *depressus* ash was sampled in the Kevin type section (Loc. #7, bed 110, Cobban et al., 1976) and biostratigraphy tightly constrains correlation of this ash to the lower of a bentonite doublet in the basal part of the middle shale unit in Pueblo (see Tab. DR1.1, Fig. DR1.2). This ash, in turn, is correlated to the lower of a pair of bentonites in the basal middle shale of the Libsack core. The ash is very well constrained to the uppermost part of the *depressus* biozone and closely approximates the Coniacian-Santonian boundary. A second *depressus* ash sampled by Bill Cobban for the Obradovich (1993) study was also analyzed. It was found in association with *S. depressus* fossils at a site near Billings, MT (Loc. #6, see Tab. 1.1).

Clioscaphtes saxitonianus – In the Kevin type section the base of the zone is defined by the FAD of *Clioscaphtes saxitonianus* at bed 113 (Grifi et al., 2012) and the top is placed just below the FAD of *Clioscaphtes vermiformis* (USGS Mesozoic locality 21665: Cobban et al., 1976). The zone is similarly constrained in Pueblo. No ashes were sampled in the zone.

Clioscaphtes vermiformis – In the Kevin type section fossils of *Clioscaphtes vermiformis* occur in the section from bed 141 through 156 (USGS Mesozoic locality D1246 is the uppermost: Cobban et al., 1976). In the Pueblo section, *C. vermiformis* is constrained to a thin zone at the top of the middle shale (USGS Mesozoic locality D3500: Scott and Cobban, 1964) that is underlain by strata containing *C. saxitonianus* and overlain by beds containing

Clioscaphtes choteauensis (USGS Mesozoic localities D2692 and D3501, respectively: Scott and Cobban, 1964). This interval is correlated to the Libsack core by lithostratigraphy. The *vermiformis* ash was not sampled in the Kevin type section, but rather at another location in Montana where *C. vermiformis* fossils were found (Loc. #4, Tab. DR1.1, Fig. DR1.2) and cannot be placed precisely within the biozone; its correlation carries a geologic uncertainty equal to the entire biozone. Given the very short duration of the zone, however, this term is minor and the *vermiformis* age provides one of the most precise anchors for the Libsack astrochronology.

Clioscaphtes choteauensis – The base of the zone in the Kevin section is placed above the LAD of *C. vermiformis*. *Clioscaphtes choteauensis* taxa occur in bed 171 (USGS Mesozoic locality D1237: Cobban et al., 1976) and the top of the zone is placed above this and just below the FAD of *Desmoscaphtes erdmanni* within bed 172 (USGS Mesozoic locality 20299: Cobban et al., 1976). The index taxon is known from Pueblo from a single specimen, taken as the base of the zone. The FAD of *Cordiceramus muelleri* (indicated as *Inoceramus simpsoni* by Scott and Cobban, 1964), higher in the upper chalky shale (Walaszczyk and Cobban, 2006), approximates the top of the zone. No ashes were sampled in the zone.

Desmoscaphtes erdmanni – Occurrences of *Desmoscaphtes erdmanni* in beds 172 and 186 of the Kevin type section (USGS Mesozoic localities 20299 and 21419, respectively: Cobban et al., 1976) define the lower and upper boundaries of the biozone. Its correlation to Pueblo is not well constrained at the top, but the base can be placed at the FAD of *C. muelleri* in the upper chalky shale unit. An ash bed was sampled at the upper boundary of the *D. erdmanni* zone in the Marias River section (Loc. #3, Tab. DR1.1, Fig. DR1.2) and this horizon is projected into the Kevin type section as shown in Figure 2 of the text. Although the ash bed occurs right at the upper boundary of the biozone, this boundary is not well constrained by fossil data in Pueblo.

Therefore, an uncertainty term equal to half the duration of the biozone is assigned to the correlation.

Desmoscaphites bassleri (+ *Scaphites leei* II) – The lower boundary of the biozone is placed at the base of the Telegraph Creek Formation in the Marias River section of Landman and Cobban (2007), and just below this is the LAD of *D. erdmanni* (USGS Mesozoic locality D21419). *Desmoscaphites bassleri* and *Haresciceras mancosense* (USGS Mesozoic locality D21420) occur a few meters above. The upper boundary of the zone is placed between the *D. bassleri* level and sample horizon D20774 (Landman and Cobban, 2007), which contains *H. montanaense*, indicating the *Scaphites leei* III zone. The *D. bassleri* zone in Pueblo is not well constrained at the base, but the top is placed just below the LOD of *Platyceramus* sp. (USGS Mesozoic locality D3509: *Platyceramus platinus* of Scott and Cobban, 1964). A *bassleri* ash was sampled in a different Montana section that contained the zone fossil (Loc. #2, Tab. DR1.1, Fig. DR1.2), but its location cannot be precisely placed in the Marias River section shown in text Figure 2. An uncertainty term equal to the entire estimated duration of the *bassleri* zone is therefore associated with its correlation to the Libsack record.

Basal Campanian and *Scaphites hippocrepis* II/*Haresciceras placentiforme* – Stratigraphic units overlying the Telegraph Creek Formation include the Virgelle Sandstone, which grades (and youngs) eastwards to the Eagle Sandstone. The Eagle Sandstone contains *Scaphites hippocrepis* II and *Haresciceras placentiforme* (Cobban, 1964, 1969) and an ash bed sampled and dated from within this zone provides a minimum age for the study interval (Loc. #1, Tab. DR1.1, Fig. DR1.2). The presence of *H. placentiforme* in the upper part of the upper chalky shale in Pueblo (USGS Mesozoic locality D3266: Scott and Cobban, 1964) facilitates correlation of this date, and is constrained above by *Haresciceras natronense* in basal beds of the upper chalk

near Boulder, CO (presumably equivalent to Libsack UC). The interval between top *bassleri* and base *placentiforme* is labeled simply “Basal Campanian” due to lack of zone fossils.

Part 3. U-Pb zircon geochronology.

DR 3.1. U-Pb methods and data interpretation

All zircons analyzed in this study employed the protocol and data reduction parameters outlined in Meyers et al. (2012), two important points are outlined here: (1) prior to dissolution zircons were subject to a modified chemical abrasion pre-treatment for the effective elimination of Pb loss (Mattinson 2005); (2) the accuracy of the $^{238}\text{U}/^{206}\text{Pb}$ dates presented herein is controlled by the gravimetric calibration of the EARTHTIME U-Pb tracer employed in this study and the determination of the ^{238}U decay constant (Condon et al. 2007; Jaffey et al. 1971). Results are summarized in Table DR 2.2 and their interpretation is discussed in this section.

For each sample between eleven and twenty single crystal/fragment U-Pb dates were determined, with each sample returning a spread in dates that exceeds the analytical precision on the single data point. There are two possible reasons for this: (1) real age variation with the sample containing zircons formed at/close to the eruption and/or prior to eruption of the ash (i.e., antecrystic or xenocrystic zircons (Miller et al., 2007); and/or (2) post-crystallization Pb-loss. Differentiating these potential controls on the U-Pb date variation is required in order to extract information that is pertinent to the age of the ash beds sampled.

In this study we have used a combination of morphology and cathodoluminescence (CL) imaging (Figure DR 2.2), in conjunction with a development moderate-*n* dataset, to guide the sampling of the youngest zircon. All zircons have undergone the chemical abrasion pre-treatment in order to minimize the occurrence of Pb-loss. Many studies have demonstrated that this method is highly effective in producing highly concordant data that represent analyses of closed system materials, however minor occurrences of Pb-loss can occur. When Pb-loss has been identified in CA-ID-TIMS data it typically manifests as a single data point that is younger than the main population thought to represent zircons crystallized at eruption. Less frequently a number of analyses will be inferred to record Pb-loss however they will show scatter with non-

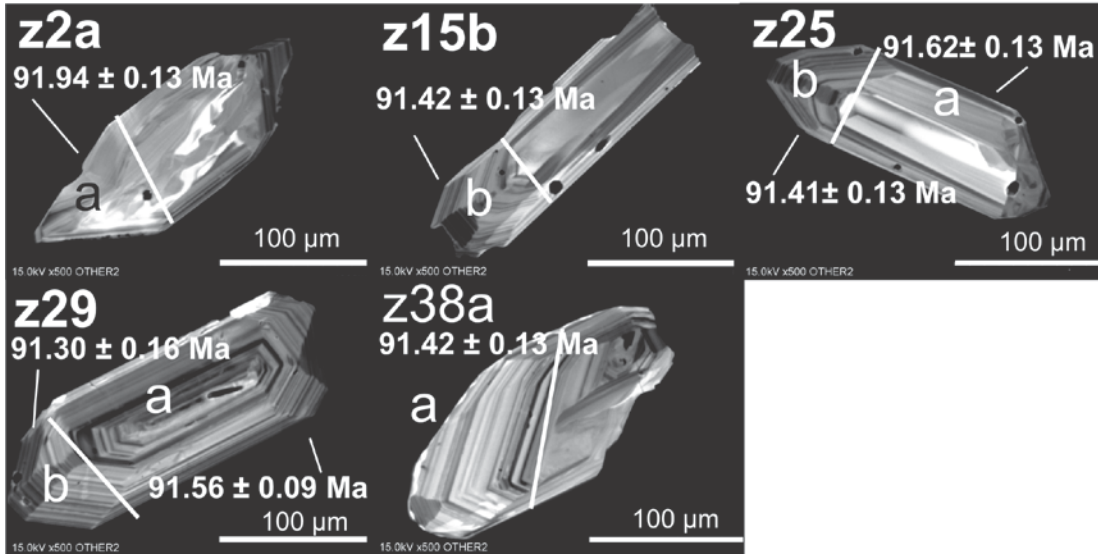
overlapping U-Pb dates reflecting the non-systematic magnitude of Pb-loss. As such we use the coherence of a data set as a measure of whether those analyses reflect a meaningful (i.e., U-Pb is closed system) population and negates any confusion between youngest U-Pb date and youngest zircon.

Using these guidelines we base our interpreted U-Pb data on a coherent population of youngest U-Pb dates. The inference is that the youngest population will not reflect any open-system behavior, and that older dates represent the incorporation of older pre-eruptive zircon. Selection of the youngest population is necessarily subjective and statistical parameters (MSWD, probability of fit) can be used as a guide, however these are dependent upon the precision of the single data point analyses. We interpreted U-Pb (zircon) ages based upon a population ($n > 4$, up to 7) of the youngest precise ^{238}U - ^{206}Pb dates using the probability of fit as a guide. Alternative interpretation, involving the incorporation of more data points, are permissible and we explore these in figure DR2.5 which shows weighted mean date/uncertainties for increasing n . The plots show that including more data points increases the weighted mean ^{238}U - ^{206}Pb date and impact the calculated uncertainty but the probability of fit rapidly decreases. Importantly, CL imaging and sub-sampling of a number of zircons indicates that some of the intra-sample variation represents intra-zircon age variation. Where core-overgrowth relationships were observed and both portions dated the overgrowth are younger by ca. 200 to 300 ka.

Importantly, the alternative (lower probability) interpreted ^{238}U - ^{206}Pb dates are not significantly different to our preferred (higher probability) dates and have minimal impact on our comparison of the ^{238}U - ^{206}Pb and $^{40}\text{Ar}/^{39}\text{Ar}$ ages.

Figure DR. 3.2. Cathodoluminescence images of selected zircons or fragments analyzed.
 The number in the upper left corner and the letter “a” or “b” correspond to the zircon or fragment analyzed in Table DR. 2.1.

UT-08-03



MT-08-01

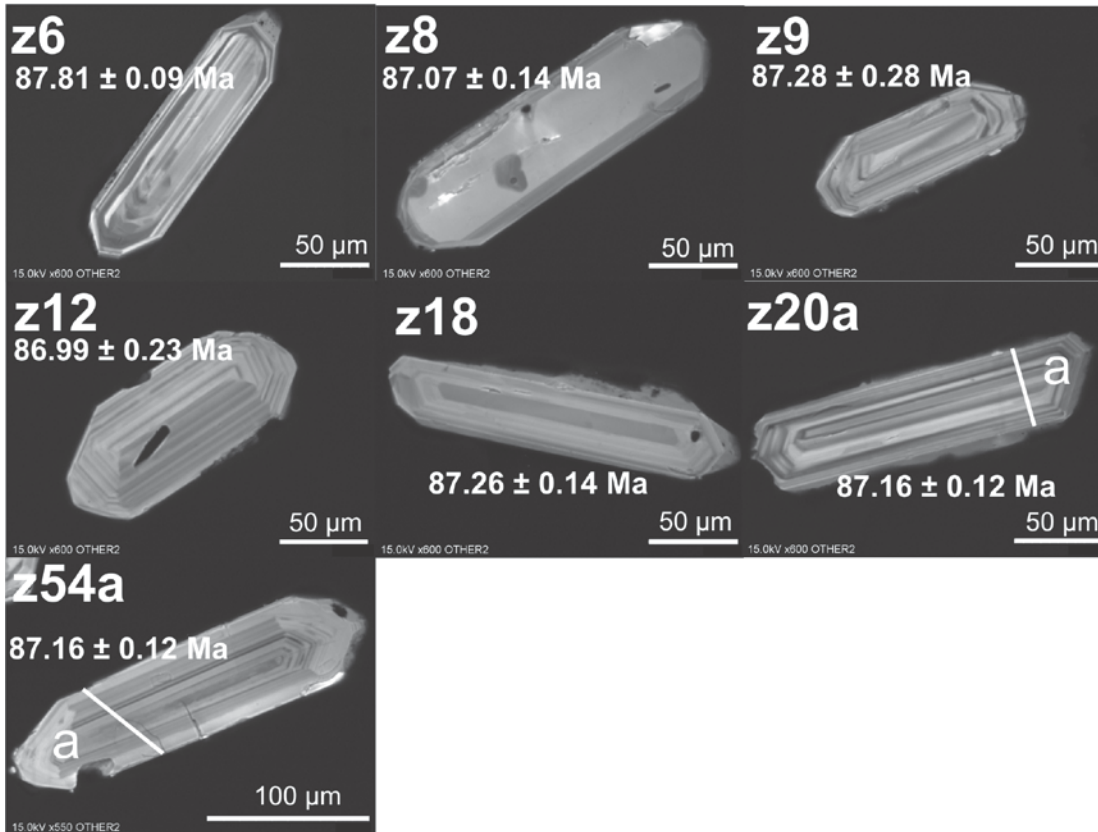


Figure DR. 3.2. (continued)

MT-08-03



Table DR 3.3. U-Pb isotope data from analyzed zircons in Cretaceous ash beds.

Fraction (a)	Radiogenic Isotope Ratios											Isotopic Ages								
	Th U	²⁰⁶ Pb* mol %	²⁰⁷ Pb* mol %	Pb* Pb _c	Pb _i (pg)	²⁰⁶ Pb (d)	²⁰⁶ Pb (e)	²⁰⁷ Pb (e)	% err (f)	²⁰⁶ Pb (e)	²⁰⁷ Pb (e)	% err (f)	corr. coef.	²⁰⁶ Pb (g)	²⁰⁷ Pb (f)	²⁰⁶ Pb (g)	²⁰⁷ Pb (f)	²⁰⁶ Pb (g)	²⁰⁷ Pb (f)	
	(b)	(c)	(c)	(c)	(c)	(e)	(e)	(f)	(e)	(e)	(f)	(e)	(f)	(g)	(f)	(g)	(f)	(g)	(f)	
UT-08-3																				
z1	2.116	0.8279	98.81%	25	0.83	1530	0.143	0.047912	0.280	0.094613	0.340	0.014322	0.097	0.703	92.55	6.64	91.79	0.30	91.76	0.09
z2a	1.632	0.5135	92.61%	4	3.39	248	0.173	0.047973	0.979	0.094923	1.061	0.014351	0.140	0.631	95.67	23.16	92.08	0.93	91.94	0.13
z3	1.152	0.3947	98.55%	23	0.48	1256	0.307	0.047919	0.327	0.094803	0.385	0.014349	0.094	0.692	93.37	7.75	91.97	0.34	91.91	0.09
z4	1.380	0.5482	99.26%	40	0.34	2466	0.142	0.047933	0.198	0.094184	0.262	0.014251	0.088	0.805	93.56	4.69	91.39	0.23	91.31	0.08
z5	0.611	0.2339	97.87%	13	0.42	853	0.132	0.047713	0.470	0.093949	0.529	0.014281	0.106	0.630	82.66	11.14	91.18	0.46	91.50	0.10
z15b	0.457	0.1636	95.96%	7	0.57	451	0.139	0.047580	0.884	0.093607	0.957	0.014269	0.143	0.567	76.03	21.00	90.86	0.83	91.42	0.13
z25a	2.327	0.9143	98.87%	26	0.87	1613	0.140	0.047794	0.365	0.094228	0.427	0.014299	0.139	0.577	86.69	8.66	91.43	0.37	91.62	0.13
z25b	0.917	0.3618	98.86%	26	0.35	1597	0.135	0.048090	0.528	0.094596	0.577	0.014266	0.146	0.453	101.32	12.47	91.78	0.51	91.41	0.13
z29a	4.189	1.6896	99.61%	75	0.55	4619	0.138	0.047952	0.123	0.094479	0.203	0.014290	0.099	0.892	94.50	2.92	91.67	0.18	91.56	0.09
z29b	1.006	0.3661	96.49%	8	1.11	518	0.138	0.047765	0.893	0.093844	0.965	0.014249	0.172	0.492	85.25	21.16	91.08	0.84	91.30	0.16
z38a	1.951	0.7855	99.41%	50	0.38	3099	0.132	0.047958	0.198	0.094346	0.256	0.014268	0.094	0.734	94.79	4.68	91.54	0.22	91.42	0.08
MT-08-3																				
z1	1.985	0.7135	97.41%	12	1.57	704	0.194	0.047803	0.545	0.092124	0.607	0.013977	0.114	0.604	87.25	12.93	89.48	0.52	89.56	0.10
z2	0.597	0.1749	93.92%	5	0.94	299	0.346	0.047610	1.651	0.092403	1.760	0.014076	0.161	0.698	78.10	39.21	89.74	1.51	90.18	0.14
z3	0.657	0.1954	91.82%	4	1.45	222	0.223	0.047261	2.716	0.091136	2.877	0.013986	0.296	0.583	60.25	64.69	88.56	2.44	89.62	0.26
z25b	1.118	0.4294	97.88%	14	0.77	860	0.128	0.047759	0.482	0.092004	0.549	0.013972	0.145	0.569	84.87	11.43	89.37	0.47	89.54	0.13
z84a	1.630	0.6006	97.55%	12	1.25	744	0.167	0.047992	0.568	0.092611	0.630	0.013996	0.132	0.554	96.50	11.43	89.93	0.54	89.69	0.12
z84b	1.716	0.6556	98.39%	18	0.89	1130	0.155	0.047937	0.353	0.092387	0.412	0.013978	0.097	0.681	93.78	8.35	89.72	0.35	89.57	0.09
z36	0.843	0.2983	96.53%	8	0.89	524	0.177	0.047740	1.060	0.091713	1.119	0.013933	0.236	0.346	84.05	25.15	89.10	0.95	89.29	0.21
z80	2.610	1.0350	99.04%	30	0.84	1888	0.136	0.047965	0.243	0.092325	0.314	0.013960	0.125	0.702	95.07	5.76	89.67	0.27	89.46	0.11
z7	0.503	0.1730	95.83%	7	0.62	436	0.186	0.047589	0.878	0.092382	0.954	0.014079	0.144	0.579	76.61	20.86	89.72	0.82	90.21	0.13
z8	0.797	0.2335	90.28%	3	2.09	187	0.174	0.048129	1.918	0.093650	2.043	0.014112	0.208	0.632	103.33	45.33	90.90	1.78	90.43	0.19
z10	1.123	0.3790	96.32%	8	1.20	494	0.234	0.047911	0.817	0.091984	0.896	0.013924	0.181	0.518	92.70	19.35	89.35	0.77	89.22	0.16
z77	3.290	0.6738	76.77%	1	16.78	80	0.112	0.048245	2.535	0.093179	2.659	0.014008	0.484	0.341	108.79	59.85	90.46	2.30	89.77	0.43
z40	0.697	0.2726	98.58%	20	0.33	1277	0.134	0.047934	0.371	0.093450	0.429	0.014139	0.102	0.648	93.58	8.79	90.71	0.37	90.60	0.09
z35	0.661	0.2225	95.59%	7	0.85	413	0.207	0.047914	1.130	0.092134	1.203	0.013946	0.169	0.486	92.80	26.77	89.49	1.03	89.36	0.15
z8b	1.230	0.4776	98.86%	26	0.46	1595	0.155	0.047754	0.291	0.093176	0.361	0.014151	0.123	0.686	84.72	6.90	90.46	0.31	90.68	0.11
z79	0.564	0.2338	98.54%	19	0.29	1247	0.063	0.048629	0.406	0.125344	0.462	0.018694	0.107	0.612	127.99	9.55	119.90	0.52	119.50	0.13
z82a	0.335	0.1197	95.65%	6	0.45	418	0.126	0.048043	0.945	0.093545	1.021	0.014122	0.132	0.617	98.92	22.34	90.80	0.89	90.49	0.12
z82b	0.817	0.3101	97.66%	12	0.62	777	0.134	0.047809	0.494	0.093493	0.556	0.014183	0.113	0.619	87.39	11.71	90.75	0.48	90.88	0.10
z8A	1.326	0.4690	95.57%	6	1.80	411	0.137	0.047492	1.119	0.092145	1.202	0.014072	0.147	0.613	71.58	26.59	89.50	1.03	90.17	0.13
MT-08-1																				
z1	1.183	0.3396	92.13%	4	2.40	232	0.298	0.047718	1.437	0.089796	1.536	0.013648	0.174	0.605	83.29	34.10	87.31	1.29	87.46	0.15
z6	0.949	0.3331	97.56%	13	0.69	747	0.231	0.047968	0.518	0.090622	0.578	0.013702	0.102	0.638	95.48	12.26	88.08	0.49	87.81	0.09
z7	1.874	0.6748	97.48%	12	1.45	721	0.194	0.047738	0.507	0.089723	0.566	0.013631	0.099	0.651	83.97	12.02	87.25	0.47	87.37	0.09
z8	0.659	0.2219	95.70%	7	0.83	424	0.211	0.047533	0.966	0.089488	1.044	0.013654	0.159	0.552	73.78	22.95	87.03	0.87	87.51	0.14
z9	2.308	0.8505	98.21%	17	1.29	1017	0.194	0.047855	0.382	0.089611	0.439	0.013581	0.096	0.668	89.75	9.05	87.14	0.37	87.05	0.08
z3	1.107	0.3390	91.47%	3	2.62	214	0.161	0.048179	1.331	0.091722	1.428	0.013807	0.154	0.659	105.67	31.44	89.11	1.22	88.49	0.14
z4	0.749	0.2631	97.18%	11	0.63	645	0.214	0.048132	0.610	0.090663	0.703	0.013661	0.242	0.531	103.50	14.41	88.12	0.59	87.55	0.21
z8.2	1.348	0.4097	95.17%	7	1.73	377	0.342	0.047638	0.979	0.089250	1.061	0.013588	0.167	0.550	79.42	23.24	86.80	0.88	87.07	0.14
z9.2	0.947	0.3075	94.18%	5	1.58	313	0.196	0.047791	1.265	0.089736	1.378	0.013618	0.322	0.452	86.60	29.99	87.26	1.15	87.28	0.28
z54a	1.312	0.4766	98.91%	29	0.43	1674	0.242	0.047877	0.344	0.089697	0.409	0.013588	0.156	0.577	91.02	8.14	87.22	0.34	87.08	0.13
z20a	1.575	0.5766	98.95%	30	0.51	1741	0.233	0.047894	0.257	0.089811	0.335	0.013600	0.144	0.693	91.79	6.09	87.33	0.28	87.16	0.12
z18	0.499	0.1815	97.26%	11	0.43	663	0.172	0.047527	0.621	0.089214	0.695	0.013614	0.160	0.550	73.40	14.76	86.77	0.58	87.26	0.14
z12	0.883	0.3272	98.00%	15	0.55	911	0.177	0.048257	1.297	0.090304	1.331	0.013572	0.270	0.226	109.52	30.62	87.79	1.12	86.99	0.23
MT-08-4																				
z4	1.089	0.4196	98.89%	27	0.39	1636	0.165	0.047873	0.257	0.087197	0.321	0.013210	0.105	0.715	90.48	6.09	84.89	0.26	84.69	0.09
z7	0.682	0.2626	98.09%	15	0.42	952	0.132	0.048068	0.414	0.087475	0.476	0.013199	0.114	0.628	99.99	9.79	85.15	0.39	84.62	0.10
z8	1.494	0.5859	99.31%	44	0.34	2856	0.160	0.048004	0.206	0.087499	0.278	0.013220	0.121	0.734	96.95	4.88	85.17	0.23	84.75	0.10
z10	1.024	0.3876	98.34%	18	0.54	1093	0.164	0.047945	0.363	0.087060	0.420	0.013170	0.093	0.681	94.05	8.58	84.76	0.34	84.43	0.08
z11	0.726	0.2623	96.50%	8	0.79	520	0.148	0.048085	0.752	0.087236	0.819	0.013158	0.115	0.631	100.88	17.77	84.92	0.67	84.36	0.10
z12	0.793	0.2230	88.26%	2	2.46	156	0.143	0.												

DR 3.4. ^{238}U - ^{206}Pb and $^{40}\text{Ar}/^{39}\text{Ar}$ data pairs

In this study we use paired ^{238}U - ^{206}Pb (zircon) and $^{40}\text{Ar}/^{39}\text{Ar}$ (sanidine) for seven samples in order to evaluate the suitability of $^{40}\text{Ar}/^{39}\text{Ar}$ data reduction parameters (FCs age, ^{40}K decay constants) in order to derive age data that are self-consistent and are considered to be accurate. The ^{238}U - ^{206}Pb (zircon) and $^{40}\text{Ar}/^{39}\text{Ar}$ (sanidine) paired datasets derived in this study are non-simple and fail to meet some of the criteria put forward for ^{238}U - ^{206}Pb and $^{40}\text{Ar}/^{39}\text{Ar}$ inter-calibration (Renne et al., 2010; Schoene et al., 2006) due to the protracted zircon crystallization implied by the U-Pb data. However, considering that the U-Pb zircon data are accurate and not perturbed by Pb-loss (see section DR 2.1.) they can be used to delineate the permissible $^{40}\text{Ar}/^{39}\text{Ar}$ age interval assuming that $^{40}\text{Ar}/^{39}\text{Ar}$ dates from sanidine should be equivalent to, or younger than, the U-Pb zircon dates. Equivalent U-Pb (zircon) and $^{40}\text{Ar}/^{39}\text{Ar}$ (sanidine) dates implies that both approximate the eruptive event, whereas $^{40}\text{Ar}/^{39}\text{Ar}$ (sanidine) younger than U-Pb (zircon) would imply that zircons crystallized and become closed systems prior to eruption. $^{40}\text{Ar}/^{39}\text{Ar}$ (sanidine) older than U-Pb (zircon) dates are not permissible in this situation given considerations of the closure temperature for both systems.

Figure 5 (main text) and Table DR 2.5 plot the U-Pb dates against the $^{40}\text{Ar}/^{39}\text{Ar}$ (sanidine) relative to FCs at 28.02, 28.201 and 28.294 Ma (using the associated decay constants and calculation methods outlined in the main text). Although the $^{40}\text{Ar}/^{39}\text{Ar}$ dates using the three different FCs ages overlap at the 95% confidence level, and each overlap with the U-Pb zircon dates, there is a systematic bias between the U-Pb and $^{40}\text{Ar}/^{39}\text{Ar}$ dates when the latter are calculated relative to 28.294 Ma FCs (Renne et al., 2011), with the U-Pb dates being younger (see Table DR 2.4).

Our findings suggest for the Cretaceous ash beds that are the focus of this study, the FCs age of 28.201 Ma and total ^{40}K decay constant of $5.463 \pm 0.214 \times 10^{-10} \text{ a}^{-1}$ (Min et al., 2000) results in a

parsimonious integrated radio-isotopic age model. The agreement between the $^{40}\text{Ar}/^{39}\text{Ar}$ (sanidine) and U-Pb zircon, coupled with the accuracy of the U-Pb system leads us to infer our age model for the stage boundaries is accurate at the stated levels of uncertainty.

Table DR. 3.5. Differences between U-Pb (zircon) and $^{40}\text{Ar}/^{39}\text{Ar}$ (sanidine) dates relative to FCs using the value of Renne et al. (1998)/Channell et al. (2010), Kuiper et al (2008) and Renne et al. (2010, 2011). Note that although the $^{40}\text{Ar}/^{39}\text{Ar}$ (sanidine) relative to FCs at 28.294 Ma and U-Pb (zircon) dates overlap at the 95% confidence level the $^{40}\text{Ar}/^{39}\text{Ar}$ dates are systematically older.

	FCs @28.02 ¹		FCs @28.201		FCs @28.294	
	Δt (ka) ²	\pm (ka) ³	Δt (ka) ¹	\pm (ka) ²	Δt (ka) ¹	\pm (ka) ²
UT-08-3	-810	405	-190	364	80	208
MT-08-3	-619	432	-9	362	241	212
MT-08-1	-576	425	14	390	264	259
MT-08-4	-621	415	-51	373	199	251
NE-08-1	-613	458	27	456	288	239
AZLP-08-1	-344	457	293	384	570	352
AZLP-08-4	-811	455	-171	412	98	297

1. Renne et al. (1998) value using a reduced uncertainty (0.67%) based upon Channell et al., (2010) and Singer et al. (2009). See text for further discussion.

2. $\Delta t = ^{40}\text{Ar}/^{39}\text{Ar}$ date - $^{206}\text{Pb}/^{238}\text{U}$ date

3. Uncertainty derived from quadratic addition of uncertainty in both $^{40}\text{Ar}/^{39}\text{Ar}$ date and $^{206}\text{Pb}/^{238}\text{U}$ dates.

Figure DR 3.6. Plot showing probability of fit for various combinations of ^{238}U - ^{206}Pb zircon dates, as well as the $^{40}\text{Ar}/^{39}\text{Ar}$ ages calculated relative to three different standard ages discussed in the text.

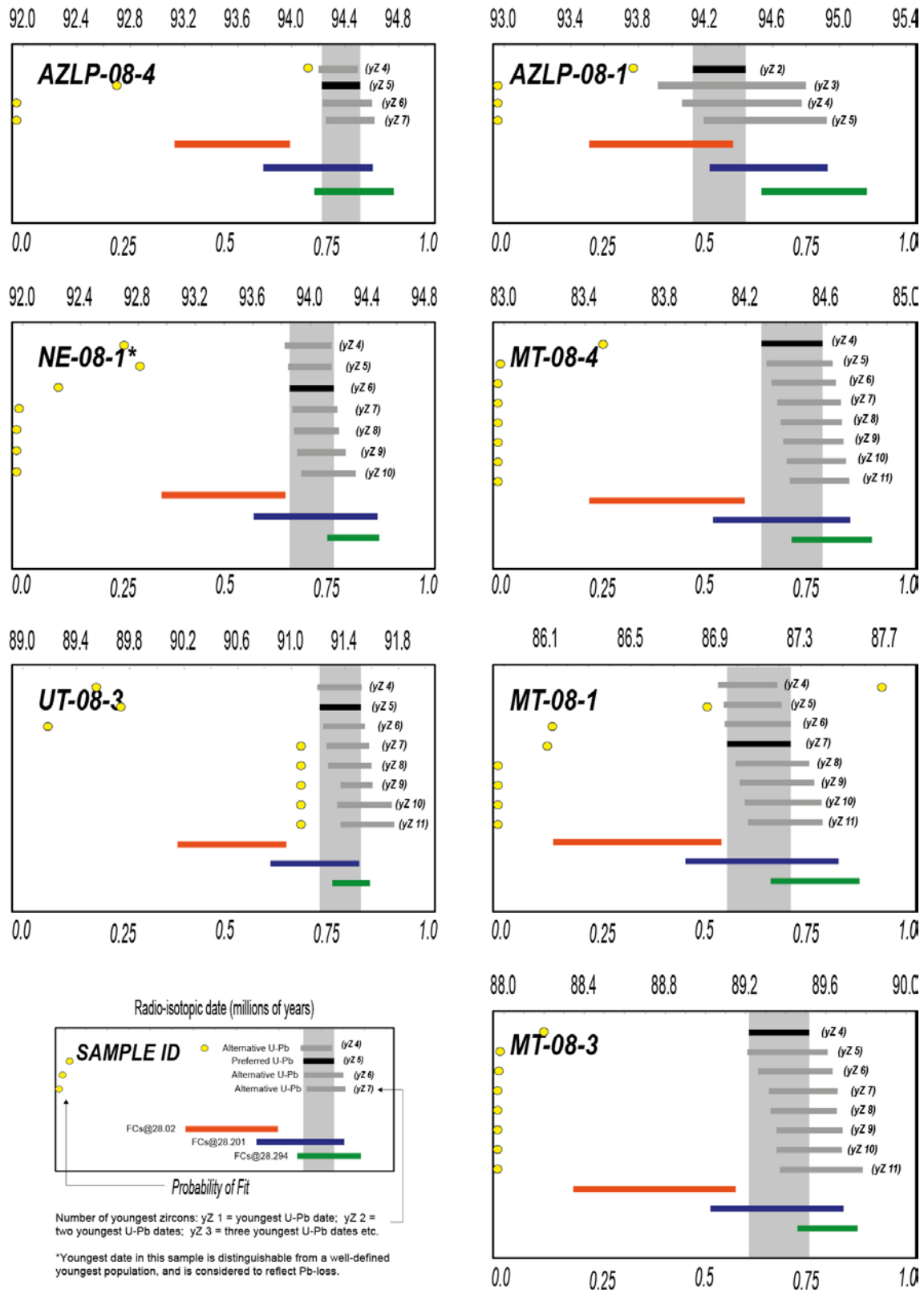
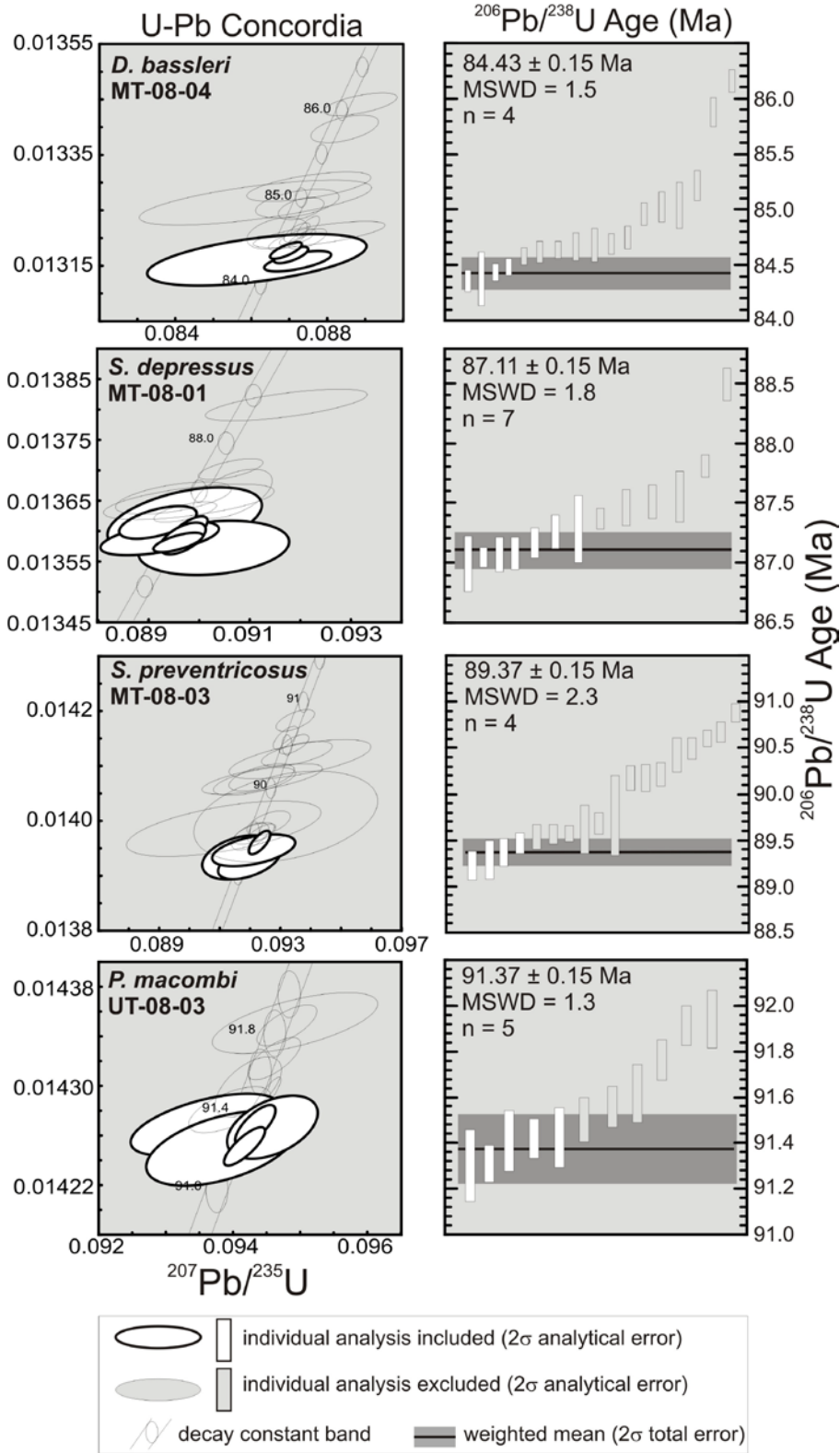


Figure DR 3.7. Concordia plots of U-Pb zircon analyses and $^{206}\text{Pb}/^{238}\text{U}$ dates.



Part 4. Argon geochronology.

DR 4.1. $^{40}\text{Ar}/^{39}\text{Ar}$ methods.

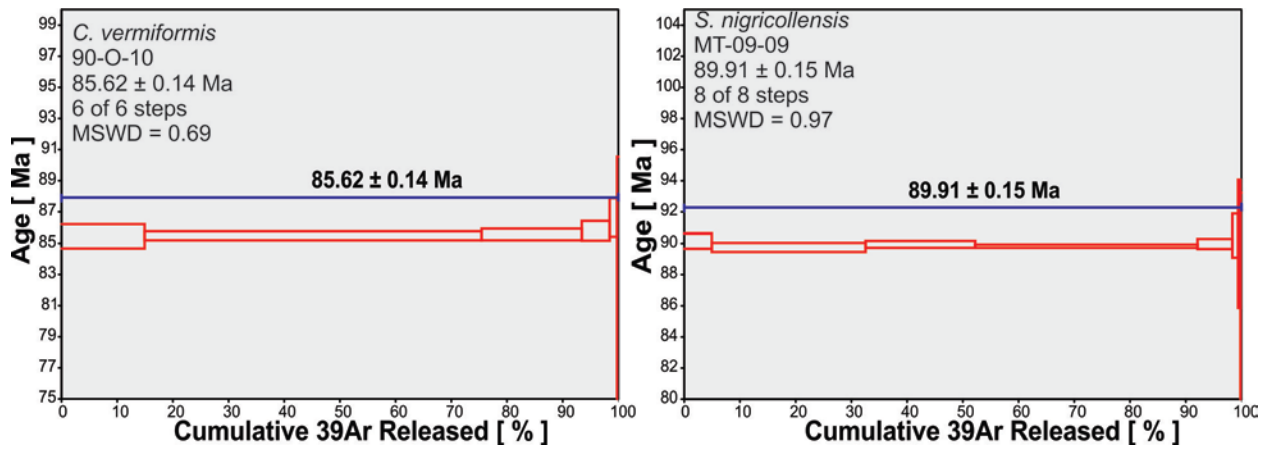
Sanidine grains were loaded into aluminum packets and placed into 1.5 cm diameter aluminum discs and co-irradiated with flux monitors for 80 hrs (experiments UW76; UW84; UW89) at the Oregon State University TRIGA reactor in the Cadmium-Lined In-Core Irradiation Tube (CLICIT) where they received a fast-neutron dose of $\sim 8 \times 10^{18} \text{ cm}^{-2}$. Fish Canyon Tuff sanidine (FCs) crystals were used as the primary neutron fluence monitor. To minimize uncertainties associated with the J-value (neutron fluence parameter), ten grains of FCs were placed directly in wells with each unknown. At the University of Wisconsin-Madison Rare Gas Geochronology Laboratory, sanidine samples and standards were fused using a 25 W CO_2 laser following the methods of Smith et al. (2008) and Meyers et al. (2012). From samples 90-O-10 (*C. vermiformis* biozone) and MT-09-09 (*S. nigricollensis* biozone), multi-crystal subsamples were also incrementally heated in 6 to 8 steps using the CO_2 laser to evaluate possible effects of alteration. Mass discrimination was assessed by analyzing the $^{40}\text{Ar}/^{36}\text{Ar}$ ratio in air pipette aliquots throughout an analytical session and were normalized to $^{40}\text{Ar}/^{36}\text{Ar} = 295.5$ (Steiger and Jäger, 1977). Two analytical sessions were required to measure the samples from irradiation UW76. During the longer session, 46 measurements of air yielded a mean mass discrimination of 1.0000 ± 0.0003 (1σ) per amu. During the shorter session 16 measurements of air gave a mean mass discrimination of 1.0016 ± 0.0002 per amu. Similarly, 47 air measurements throughout the analytical session devoted to the UW84 irradiation yield a mean mass discrimination of 1.0033 ± 0.0002 per amu. A short session to reanalyze two sanidine separates from the UW89 irradiation resulted in a mass discrimination of 1.0053 ± 0.0001 . The differences in the mass discrimination from UW76 to UW89 is likely attributed to slight modifications to the mass spectrometer tuning conditions.

In our previous studies (Smith et al., 2008; Meyers et al., 2012), the t_0 intercept for each mass of Ar was determined by regressing a line or exponential curve through the mean signal size of the ion beam integrated during 8 cycles through the mass range. However the ^{40}Ar and ^{39}Ar peaks are measured 5 times each during ~10 seconds of counting whereas ^{36}Ar is measured 20 times during 32 seconds of counting in each peak cycle. Rather than regressing 8 measurements for each argon mass to constrain the signal size, the procedure used in the present study considers all raw peak signals collected during each cycle. This facilitates removal of outliers that may reflect electronic noise, and results in a far greater number of data points available to constrain the slope and intercept of the regressed curve for each argon mass. This procedure results in more precise estimates of the t_0 intercepts and in turn more precise ages for samples with comparable signal sizes than we have reported in our previous studies. To facilitate comparison of ages, the raw signal data from samples NE-08-01, AZLP-08-04, and 90-O-30 (equivalent to AZLP-08-01) of Meyers et al. (2012) was re-processed using the new algorithm and these data are presented along with all the data collected for this study in Table DR 3.2 (Excel spreadsheet).

Table DR 4.2.

See separate Excel spreadsheet file for the complete $^{40}\text{Ar}/^{39}\text{Ar}$ isotope data from samples and standard minerals used as neutron fluence monitors.

Figure DR 4.3. Age spectrum diagrams from incremental heating analyses. Data is from Table DR 3.1.



REFERENCES FOR DATA REPOSITORY

- Cobban, W.A., 1964, The Late Cretaceous cephalopod *Haresiceras* Reeside and its possible origin: U.S. Geological Survey Professional Paper 454-I, 21 p., 3 pl.
- Cobban, W.A., 1969, The Late Cretaceous ammonites *Scaphites leei* Reeside and *Scaphites hippocrepis* (DeKay) in the western interior of the United States: U.S. Geological Survey Professional Paper 619, 29 p.
- Cobban, W.A., Erdmann, C.E., Lemke, R.W., and Maughan, E.K., 1976, Type Sections and Stratigraphy of the Members of the Blackleaf and Marias River Formations (Cretaceous) of the Sweetgrass Arch, Montana: U.S. Geological Survey Professional Paper 974, 66 p.
- Cobban, W.A., Dyman, T.S., and Porter, K.W., 2005, Paleontology and stratigraphy of upper Coniacian-middle Santonian ammonite zones and application to erosion surfaces and marine transgressive strata in Montana and Alberta: *Cretaceous Research*, v. 26, no. 3, p. 429–449.
- Cobban, W.A., Walaszczyk, I., Obradovich, J.D., and McKinney, K.C., 2006, A USGS zonal table for the Upper Cretaceous middle Cenomanian-Maastrichtian of the Western Interior of the United States based on ammonites, inoceramids, and radiometric ages: U.S. Geological Survey Open-File Report OF 2006-1250, 46 p.
- Crowley, J.L., Schoene, B., and Bowring, S.A., 2007, U-Pb dating of zircon in the Bishop Tuff at the millennial scale: *Geology*, v. 35, p. 1123–1126.
- Endt, P.M., 1998, Supplement to energy levels of $A=21-44$ nuclei (VII): *Nuclear Physics A*, v. 633, no. 1, p. 04Fi10.
- Fisher, C. G.; Kauffman, E.G; Wilhelm, L. Von Holdt, 1985, The Niobrara transgressive hemicyclothem in central and eastern Colorado: The anatomy of a multiple disconformity: *SEPM Guidebook*, v. 4, p. 184–198.
- Grifi, M.D., Plint, A.G., and Walaszczyk, I., 2013, Rapidly changing styles of subsidence revealed by high-resolution mudstone allostratigraphy: Coniacian of Sweetgrass Arch area, southern Alberta and northern Montana, *Canadian Journal of Earth Sciences*, v. 50, p. 1–24, doi:10.1139/cjes-2012-0031.
- Gardner, M.H., 1995, The Stratigraphic Hierarchy and Tectonic History of Mid-Cretaceous foreland basin of central Utah, *in* Dorobek, S., and Ross, J., eds., *Stratigraphic Evolution of Foreland basins*: *SEPM Special Publication* 52, p. 243–283.
- Jaffey, A.H., Flynn, K.F., Glendenin, L.E., Bentley, W.C., and Essling, A.M., 1971, Precision measurement of half-lives and specific activities of ^{235}U and ^{238}U : *Physical Review*, v. C4, p. 1889–1906.
- Koppers, A.P., 2002, ArArCALC; software for $^{40}\text{Ar}/^{39}\text{Ar}$ age calculations: *Computers and Geosciences*, v. 28, no. 5, p. 605–619.
- Kuiper K.F., Deino, A., Hilgen, F.J., Krijgsman, W., Renne, P.R., and Wijbrans, J.R., 2008, Synchronizing Rock Clocks of Earth History: *Science*, v. 320, p. 500–504.

- Landman, N.H. and Cobban, W.A., 2007, Redescription of the Late Cretaceous (late Santonian) ammonite *Desmoscaphites bassleri* Reeside, 1927, from the Western Interior of North America: *Rocky Mountain Geology*, v. 42, no. 2, p. 67–94.
- Locklair, R.E., and Sageman, B.B., 2008, Cyclostratigraphy of the Upper Cretaceous Niobrara Formation, Western Interior, U.S.A.: A Coniacian-Santonian orbital timescale: *Earth and Planetary Science Letters*, v. 269, p. 540–553.
- Ludwig, K.R., 2003, User's Manual for Isoplot 3.00: A Geochronological toolkit for Microsoft Excel: Berkeley Geochronology Center Special Publication 4, 70 p.
- Mattinson, J.M., 2005, Zircon U/Pb chemical abrasion (CA-TIMS) method: *Chemical Geology*, v. 220, p. 47–66.
- Meyers, S.R., Sageman, B., and Hinnov, L., 2001, Integrated quantitative stratigraphy of the Cenomanian-Turonian Bridge Creek Limestone Member using Evolutive Harmonic Analysis and stratigraphic modeling: *Journal of Sedimentary Research*, v. 71, p. 627–643.
- Miller, J.S., Matzel, J.E.P., Miller, C.F., Burgess, S.D., and Miller, R.B., 2007, Zircon growth and recycling during the assembly of large, composite arc plutons: *Journal of Volcanology and Geothermal Research*, v. 167, p. 282–299.
- Min, K., Mundil, R., Renne, P.R., and Ludwig, K.R., 2000, A test for systematic errors in $^{40}\text{Ar}/^{39}\text{Ar}$ geochronology through comparison with U/Pb analysis of a 1.1-Ga rhyolite: *Geochimica et Cosmochimica Acta*, v. 64, p. 73–98.
- Obradovich, J., 1993, A Cretaceous time scale, *in* Caldwell, W.G.E., and Kauffman, E.G., eds., *Evolution of the Western Interior Basin: Geological Society of Canada Special Paper 39*, p. 379–396.
- Renne, P.R., and Norman, E.B., 2001, Determination of the half-life of ^{37}Ar by mass spectrometry: *Physical Review C*, v. 63, 047302-3.
- Renne, P.R., Mundil, R., Balco, G., Min, K., and Ludwig, K.R., 2010, Joint determination of ^{40}K decay constants and $^{40}\text{Ar}^*/^{40}\text{K}$ for the Fish Canyon sanidine standard, and improved accuracy for $^{40}\text{Ar}/^{39}\text{Ar}$ geochronology: *Geochimica Et Cosmochimica Acta*, v. 74, no. 18, p. 5349–5367.
- Sageman, B.B., Meyers, S.R., and Arthur, M.A., 2006, Orbital time scale and new C-isotope record for Cenomanian-Turonian boundary stratotype: *Geology*, v. 34, p. 125–128.
- Scott, G.R., and Cobban, W.A., 1964, Stratigraphy of the Niobrara Formation at Pueblo, Colorado: U.S. Geological Survey Professional Paper 454-L, 27 p.
- Schoene, B., Crowley, J. L., Condon, D. J., Schmitz, M. D., and Bowring, S. A., 2006, Reassessing the uranium decay constants for geochronology using ID-TIMS U-Pb data: *Geochimica Et Cosmochimica Acta*, v. 70, no. 2, p. 426-445.
- Schmitz, M.D., and Schoene, B., 2007, Derivation of isotope ratios, errors, and error correlations for U-Pb geochronology using ^{205}Pb - ^{235}U -(^{233}U)-spike isotope dilution thermal ionization mass spectrometric data: *Geochemistry Geophysics Geosystems*, v. 8, Q08006.

- Scott, G.R., and Cobban, W.A., 1964, Stratigraphy of the Niobrara Formation at Pueblo, Colorado: U.S. Geological Survey Professional Paper 454-L, p. 27.
- Steiger, R.H., and Jäger, E., 1977, Subcommission on Geochronology: Convention on the use of decay constants in geo- and cosmochronology: *Earth and Planetary Science Letter*, v. 36, p. 359–362.
- Stoener, R.W., Schaeffer, O.A., and Katcoff, S., 1965, Half-lives of argon-37, argon-39 and argon-42: *Science*, v. 148, p. 1325–1328.
- Walaszczyk, I., and Cobban, W.A., 2000, Inoceramid Faunas and Biostratigraphy of the Upper Turonian-Lower Coniacian of the Western Interior of the United States: *Palaeontological Association [London] Special Paper*, v. 64, 118 p.
- Walaszczyk, I., and Cobban, W.A., 2006, Palaeontology and stratigraphy of the Middle-Upper Coniacian and Santonian inoceramids of the US Western Interior: *Acta Geologica Polonica*, v. 56, p. 241–348.
- Walaszczyk, I., and Cobban, W.A., 2007, Inoceramid fauna and biostratigraphy of the upper Middle Coniacian-lower Middle Santonian of the Pueblo Section (SE Colorado, US Western Interior): *Cretaceous Research* v. 28, p. 132–142.